Chem

CellPress

Article

Reversible topochemical polymerization and depolymerization of a crystalline 3D porous organic polymer with C–C bond linkages

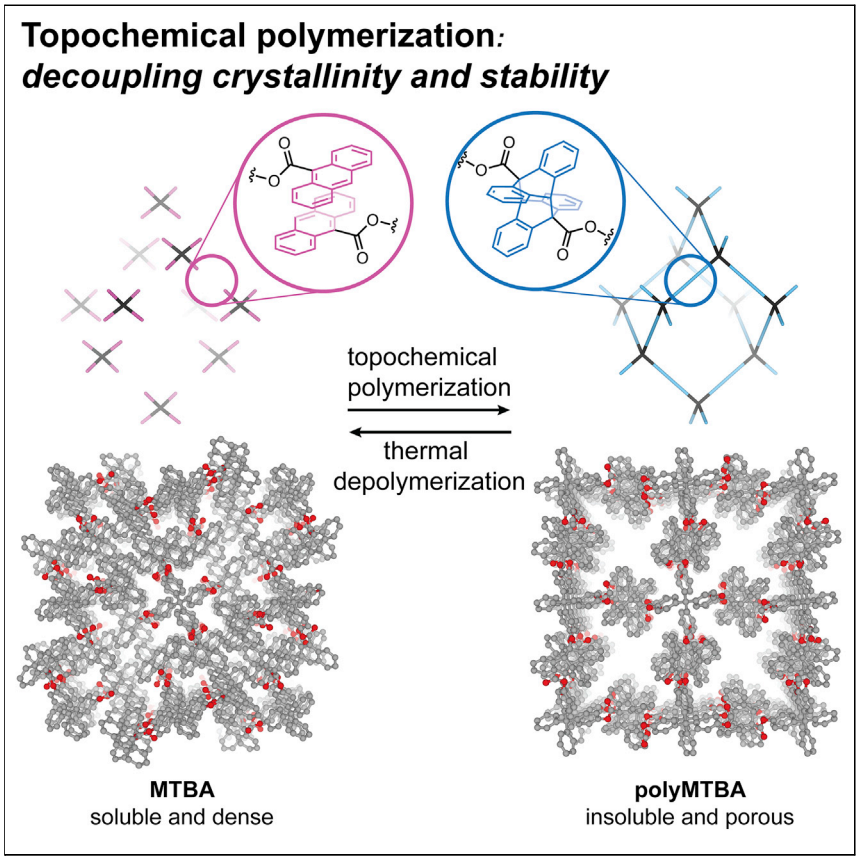

Common synthesis of organic covalent crystals entails a trade-off between stability and crystallinity, as the former impedes the error correction necessary for long-range ordering. Here, we introduce the topochemical method, where crystallization and bond formation are decoupled temporally, thus allowing the formation of stable C–C connections without sacrificing crystallinity. Using this method, a dense, soluble crystalline monomer is converted into a porous, insoluble crystalline polymer. This work opens a new avenue for functional crystalline porous organic polymer.

Chenyue Sun, Julius J. Oppenheim, Grigorii Skorupskii, Luming Yang, Mircea Dincă

mdinca@mit.edu

Highlights

Solid-state generation of C–C-linked crystalline porous organic polymer

Thermal depolymerization of the porous polymer regenerates monomer

The microporous polymer is indirectly yet readily solution processible

Sun et al., Chem 8, 1–10
December 8, 2022
https://doi.org/10.1016/j.chempr.2022.07.028

Please cite this article in press as: Sun et al., Reversible topochemical polymerization and depolymerization of a crystalline 3D porous organic polymer with C–C bond linkages, Chem (2022), https://doi.org/10.1016/j.chempr.2022.07.028

Chem

CellPress

Article

Reversible topochemical polymerization and depolymerization of a crystalline 3D porous organic polymer with C–C bond linkages

Chenyue Sun,[1] Julius J. Oppenheim,[1] Grigorii Skorupskii,[1] Luming Yang,[1] and Mircea Dincă[1,2,*]

SUMMARY

Three-dimensionally connected porous organic polymers are of interest because of their potential in adsorption, separation, and sensing, among others. When crystalline, they also afford accurate structure description, which in turn can enable particular functions. However, crystallization of three-dimensional (3D) polymers is challenging. This is especially true when targeting polymerization via stable C–C bonds, whose formation is usually irreversible and does not allow for error correction typically required for crystallization. Here, we report polyMTBA, the first 3D-connected crystalline organic polymer with permanent porosity, here formed via C–C linkages. High crystallinity is achieved by solid-state topochemical reaction within monomer MTBA crystals. polyMTBA is recyclable via thermal depolymerization and is solution processable via its soluble monomers. These results reveal topochemical polymerization as a compelling methodology for generating stable, crystalline, and porous 3D organic frameworks.

INTRODUCTION

Organic porous materials such as hypercrosslinked polymers,[1] covalent organic frameworks (COFs),[2] conjugated microporous polymers (CMPs),[3] and porous aromatic frameworks (PAFs)[4] have garnered considerable attention for their utility in adsorption,[5–9] catalysis,[10–12] and energy storage.[13–18] Among these, COFs stand out because of their crystallinity, which both allows for accurate description and understanding of their structure and confers unique benefits such as monodisperse size-selective sieving, shape selection, and control over capillary condensation.[19–21] On the other hand, CMPs, PAFs, and hypercrosslinked polymers stand out through their typically enhanced chemical stability afforded by irreversible C–C and aromatic linkages.[3,4,22,23] Despite recent advances in C=C-linked COFs,[24,25] it is still challenging to form crystalline C–C-linked porous frameworks via solvothermal routes because these require irreversible bond formation and crystallization in a single step, which is incompatible with error correction during crystal growth.

To this end, topochemical polymerization provides a promising avenue to stable, highly crystalline materials.[26] With topochemical polymerization, monomer polymorphs are chosen in such a way that the reactive functional groups are spatially aligned in close proximity to allow for bond formation in the solid state. Subsequent C–C bond formation, triggered by light or some other stimuli, is effectively decoupled from crystallization and thus gives rise to highly crystalline polymers. Although early examples of topochemical polymerization primarily focused on generating one-dimensional polymers, particularly with diynes and dienes,[26,27] in

THE BIGGER PICTURE

Covalent crystals such as silicon, quartz, and zeolites are three-dimensionally ordered arrays of atoms interconnected with solely covalent bonds. The crystallinity and covalency are key to their widespread use in both scientific and industrial settings. Organic covalent crystals, where the building blocks are organic small molecules rather than atoms, are an emerging subclass that builds upon our vast knowledge in synthetic organic chemistry. However, the solvothermal synthesis of these materials requires simultaneous covalent bond formation and crystallization, leading to a constant trade-off between crystallinity and stability of the covalent linkage. In this work, we decouple the two steps through in-crystallo topochemical dimerization and thereby generate the first three-dimensional porous organic covalent crystal with irreversibly formed C–C bond. This methodology provides a new avenue to highly stable, highly crystalline, and highly functional organic covalent materials.

Please cite this article in press as: Sun et al., Reversible topochemical polymerization and depolymerization of a crystalline 3D porous organic polymer with C–C bond linkages, Chem (2022), https://doi.org/10.1016/j.chempr.2022.07.028

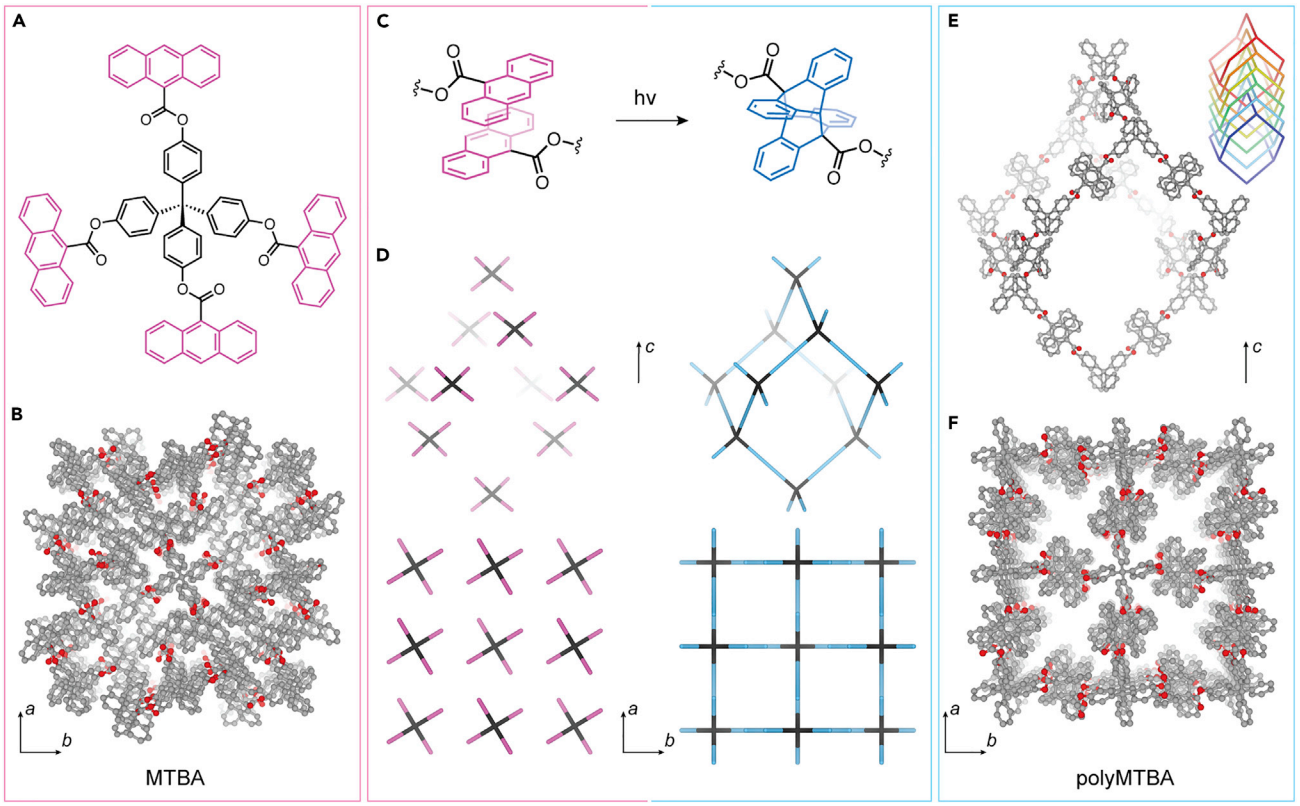

Figure 1. Structural details of MTBA and polyMTBA

(A) The molecular structure of monomer **MTBA**.

(B) Representations of the crystal structure of **MTBA** (single crystal X-ray diffraction data).

(C) adjacent anthroate pairs in crystalline **MTBA** undergo dimerization upon irradiation.

(D) Individual **MTBA** building units are pre-arranged in the crystalline phase (left); these units are then covalently linked to form the diamond-type framework in **polyMTBA** (right). A single isolated network is shown for clarity.

(E) A single adamantane-like cage in **polyMTBA**. Actual **polyMTBA** is 6-fold interpenetrated (inset).

(F) Representations of the crystal structure of **polyMTBA** (molecular mechanics model based on Pawley refinement of unit cell parameters from powder X-ray diffraction). Hydrogen atoms are omitted for clarity.

recent years, increasing efforts have been devoted to 2D polymers, taking advantage of the photochemical dimerization reaction of stilbene and anthracene derivatives.[28–32] High-pressure and high-temperature topochemical polymerization of C_{60} also produces a crystalline, non-porous material.[33,34] More recently, a hybrid approach was reported to create 3D-connected COFs by topochemically connecting preformed 2D COFs.[35–37] To our knowledge, however, topochemical transformations have not been employed yet to produce porous 3D crystalline organic polymers.

Here, we report that photochemical polymerization of methanetetrayltetrakis(benzene-4,1-diyl) tetrakis(anthracene-9-carboxylate) (**MTBA**, Figure 1A) crystals in the solid state yields a crystalline porous solid (**polyMTBA**, Figure 1F) with permanent porosity. Although **MTBA** crystals have no discernible crystallographic voids, porosity emerges in **polyMTBA** due to a large displacement of monomer molecules during polymerization, which creates one-dimensional channels along the *c*-direction (Figures 1B and 1F). **polyMTBA** can be deposited onto glass substrates from solution-processed **MTBA** films and can be thermally degraded to recover pristine monomer.

[1]Department of Chemistry, Massachusetts Institute of Technology, Cambridge, MA 02139, USA

[2]Lead contact

*Correspondence: mdinca@mit.edu

https://doi.org/10.1016/j.chempr.2022.07.028

Please cite this article in press as: Sun et al., Reversible topochemical polymerization and depolymerization of a crystalline 3D porous organic polymer with C–C bond linkages, Chem (2022), https://doi.org/10.1016/j.chempr.2022.07.028

RESULTS AND DISCUSSION

Tetratopic monomer pre-organizes within a molecular crystal

The molecular structure of **MTBA** was carefully chosen to favor a rigid and open framework structure. Anthracene is attractive as a topochemical motif because of its relatively small size and its well-documented photodimerization chemistry.[38] In particular, 9-substituted anthracenes tend to crystallize and dimerize in a head-to-tail fashion (Figure 1C). Inspiration for the tetrahedral tetraphenylmethane core in **MTBA** came from COFs,[39,40] which use this motif to impose high rigidity and maximal angular separation between the peripheral groups, which are conducive to permanent porosity. It should be noted that due to the highly congested nature around the bridgehead carbon atoms in dianthracene, the range of permissible substituents at the 9 and 10 positions of anthracene is quite limited. For instance, 9,10-diphenylanthracene is photochemically inert in both solution and solid states, likely because the ortho-H on the phenyl group prevents the proximity of two anthracene units in the transition state.[41] A sterically less-demanding ester linkage, on the other hand, does not affect the dimerization.[42]

MTBA crystallizes in the tetragonal space group $I4_1/a$ with no lattice solvent. Individual **MTBA** molecules stack into columns along the *c*-direction, collinear with the S_4 molecular axis (Figure 1D). Each anthracene group is paired face-to-face (dihedral angle <0.01°, interplanar distance 3.3–3.6 Å) with an anthracene from a neighboring molecule. However, significant slipping displacement between the two neighboring anthracene groups gives rise to a large C9···C10′ separation of 5.3–5.6 Å (Figure S1), which is much larger than what is commonly believed to be the maximal separation (4.2 Å, Schmidt criterion[43]) allowed for topochemical anthracene dimerization. However, the two neighboring anthracene groups still interact electronically and give rise to excimeric emission, as exhibited by the green photoluminescence (λ_{max} = 503 nm, Figure S2) of a polycrystalline powder of **MBTA**.

Crystal-to-crystal transformation affords 3D-connected covalent crystal

Despite the large C9···C10′ separation, irradiation of **MTBA** crystals at 370 or 427 nm induced a noticeable change of the fluorescence from intense green to faint sky-blue, whereas the solid turned from bright yellow to beige. In our hands, the most complete transformation, as assessed by adsorption capacity (*vide infra*), was obtained by irradiating a continuously stirred suspension of powder **MTBA** in diethyl ether under 1 bar of CO_2 with a 427 nm LED for 3 days. The absence of CO_2 during irradiation leads to a product exhibiting lower porosity, leading us to believe that CO_2 may fill pores generated during topochemical transformation, thereby compensating for the loss of dispersive interaction between **MTBA** molecules. Additionally, **MTBA** itself adsorbs 13.3 cm^3/g CO_2 at 1 bar and 273 K, confirming that CO_2 penetrates the monomer lattice to some extent (Figure S3). Importantly, diethyl ether does not dissolve **MTBA** and therefore serves as a good suspension medium for monomer powder, allowing for better irradiation exposure. Furthermore, 427 nm is at the edge of the absorption peak of **MTBA** (Figure S4); irradiation at this wavelength improves light penetration into the crystals.[44]

Characterization of the photoproduct suggests the emergence of a significant amount of dianthracene linkages and loss of spectroscopic features for monomeric anthracene groups. Diffuse-reflectance UV-visible spectroscopy shows significant weakening of the characteristic absorption of anthracene above 300 nm in the photoproduct (Figure S4). By diffuse-reflectance infrared Fourier-transform spectroscopy (Figure S5), **MTBA** shows no strong features in the 700–600 cm^{-1} region,

Please cite this article in press as: Sun et al., Reversible topochemical polymerization and depolymerization of a crystalline 3D porous organic polymer with C–C bond linkages, Chem (2022), https://doi.org/10.1016/j.chempr.2022.07.028

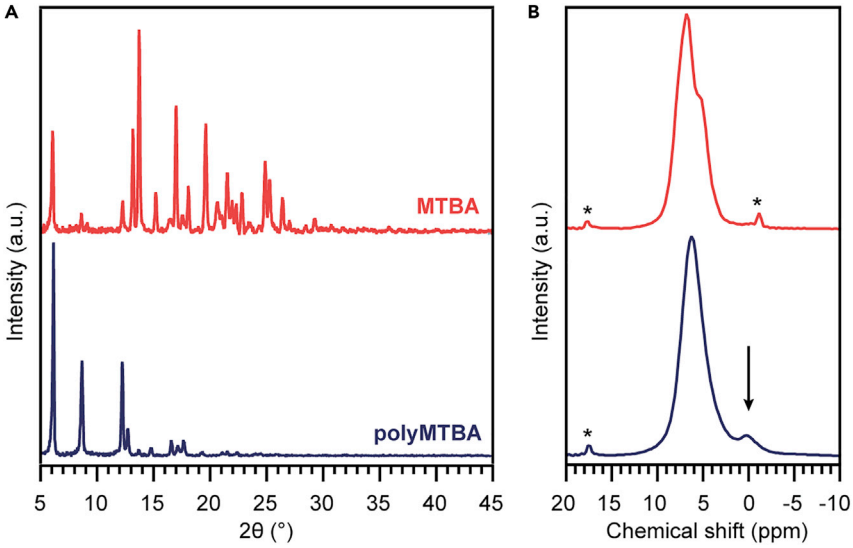

Figure 2. Qualitative and quantitative evidence for transformation from MTBA to polyMTBA
(A) Transformation is evident from significant changes in the intensity and peak positions of the powder X-ray diffraction (PXRD) patterns.
(B) Quantitative ^{1}H solid-state nuclear magnetic resonance (SS-NMR) spectra show clear appearance of the bridgehead benzylic proton (denoted by an arrow) upfield of the aromatic signals. Strong intermolecular shielding causes large upfield shifts. Asterisks denote artifact signals from sample rotor/probe. Spinning side bands are outside the spectral window presented.

whereas the photoproduct displays two strong bands at 690 and 636 cm^{-1}, characteristic of anthroate dimers.[45] A cross-polarized magic-angle spinning ^{13}C solid-state nuclear magnetic resonance (SS-NMR) spectrum of the photoproduct displays new peaks at approximately 50 ppm, which are assigned to the bridgehead carbon in dianthracene (Figure S6). Altogether, vibrational, electronic, and NMR spectroscopy along with the loss of excimeric emission confirm the dimerization of a significant portion of neighboring anthracene units in solid **MTBA**.

To quantify the degree of photopolymerization, we turned to high-resolution solid-state ^{1}H-NMR spectroscopy with homonuclear dipolar decoupling.[46] We note that in the solid state, all protons shift significantly upfield relative to the solution spectra due to the strong shielding effect of nearby aromatic rings,[47] but the benzylic proton of dianthracenes can still be readily discerned from the aromatic protons (Figure 2B). Peak integration gives a ratio of 12.8:1 aromatic to benzylic protons, which equates to up to 93% polymerization (see supplemental information for additional discussion). This high degree of photodimerization is surprising, given that the separation of anthracene units in **MTBA** seems to violate the Schmidt criterion (*vide supra*) but is by no means unprecedented and is likely enabled by significant motion of the monomers under irradiation: solid-state photodimerization reactions involving even larger molecular motions have been reported.[48,49] Indeed, the relatively slow photopolymerization in our system (days, cf. hours in Kissel et al.[29] and Kory et al.[30]) is in line with those involving significant molecular displacement. If we assume that all anthracene groups within each monomer engage in photodimerization, the photoproduct is a 3D polymer network, i.e., **polyMTBA** (Figures 1C and 1D). Consistent with this assignment, the photoproduct is insoluble in common organic solvents.

Crucially, the transformation from **MTBA** to **polyMTBA** preserves crystallinity. The powder X-ray diffraction (PXRD) pattern of **polyMTBA** is clearly distinct from that of

Please cite this article in press as: Sun et al., Reversible topochemical polymerization and depolymerization of a crystalline 3D porous organic polymer with C–C bond linkages, Chem (2022), https://doi.org/10.1016/j.chempr.2022.07.028

MTBA in both peak positions and relative intensities (Figures 2A and S8). Scanning electron microscopy (SEM) showed that the square prismatic shape of **MTBA** crystallites persists after polymerization without noticeable deformation (Figure S7). However, efforts to obtain single crystals of **polyMTBA** were unsuccessful: even when attempting photopolymerization at low temperature (223 K), single crystals of **MTBA** rapidly degrade to show only polycrystalline diffraction features. However, a combination of Pawley refinement and molecular mechanics optimization provided reliable insight into the structure of **polyMTBA** (Figures 1, **S8**, and **S9**). Thus, high-resolution synchrotron PXRD data of **polyMTBA** can be fitted well in the same $I4_1/a$ space group as the monomer, with notable expansion along both *a* (28.8432(3) Å versus 28.2999(3) Å of **MTBA**) and *c* (15.9068(2) Å versus 15.0898(2) Å of **MTBA**). Scaling the experimental crystal structure of **MBTA** accordingly and replacing the anthracene monomer pairs with dianthracenes gave a polymer model used as the input for molecular mechanics optimization. Overall, the computed fully polymerized **polyMTBA** can be viewed as a 6-fold interpenetrated diamond-type framework (Figure 1E). Importantly, one-dimensional open channels with a diameter of approximately 3.9 Å extend parallel to the *c*-direction (Figures 1F and S9).

Thanks to the solubility of **MTBA**, **polyMTBA** can be facilely processed into various forms. For instance, spin-coating of an **MTBA** solution onto glass and quartz substrates forms initially amorphous films, which transform into discrete spindle-shaped crystallites upon solvent-vapor annealing. Subsequent irradiation of this surface-deposited **MTBA** precursor led to diminished crystallinity; however, evident shifts in the grazing-incidence X-ray diffraction pattern indicate polymerization and formation of **polyMTBA** (Figure 3B) without apparent change in the crystallites (Figure 3A). Surface deposition here allows for efficient light penetration and a high degree of polymerization after irradiation (Figures 3A and S10) as evidenced by the clean disappearance of the anthracene UV-visible absorption above 300 nm (Figure 3C) and complete loss of excimeric photoluminescence (Figure 3D).

CO_2 adsorption isotherms confirmed the ultramicroporous nature of **polyMTBA**. Due to kinetic restrictions, **polyMTBA** adsorbs minimal N_2 at 77 K.[50] However, a CO_2 isotherm measured at 195 K exhibits steep uptake at low pressure and a capacity of 4.75 mmol/g (108 cm^3/g STP, 14.8 wt %) at 0.93 bar (Figure S11). At 273 K, **polyMTBA** adsorbs 1.38 mmol/g (31.3 cm^3/g STP, 4.8 wt %) at 1.0 bar (Figure S11). This capacity is very close to the value obtained from simulation on the molecular mechanics-optimized model[51] (34.2 $\pm$ 2.0 cm^3/g STP at 1.0 bar). Fitting the CO_2 isotherm at 195 K to the Brunauer-Emmett-Teller (BET) model gives an apparent surface area of 350 m^2/g (calc. 408.6 $\pm$ 0.4 m^2/g for the optimized model). The isosteric heat of adsorption at low coverage was calculated to be ~23 kJ/mol (Figure S12), on par with previously reported values for microporous carbon molecular sieves.[52]

Thermal depolymerization regenerates the monomer

Importantly, **polyMTBA** depolymerizes into **MTBA** at elevated temperature. Thermal scission of molecular dianthracene derivatives can have an onset temperature in the wide range of 90°C–200°C.[45] Thermogravimetric analysis (TGA) of **polyMTBA** and **MTBA** under inert atmosphere gives identical results, with a plateau at lower temperature and a rapid mass loss above 375°C (Figure S13). The similar thermal behavior between the monomer and the polymer is consistent with the expectation that **polyMTBA** depolymerizes below 375°C. To pinpoint the decomposition temperature, we performed variable-temperature (VT) PXRD of **polyMTBA** under a

Please cite this article in press as: Sun et al., Reversible topochemical polymerization and depolymerization of a crystalline 3D porous organic polymer with C–C bond linkages, Chem (2022), https://doi.org/10.1016/j.chempr.2022.07.028

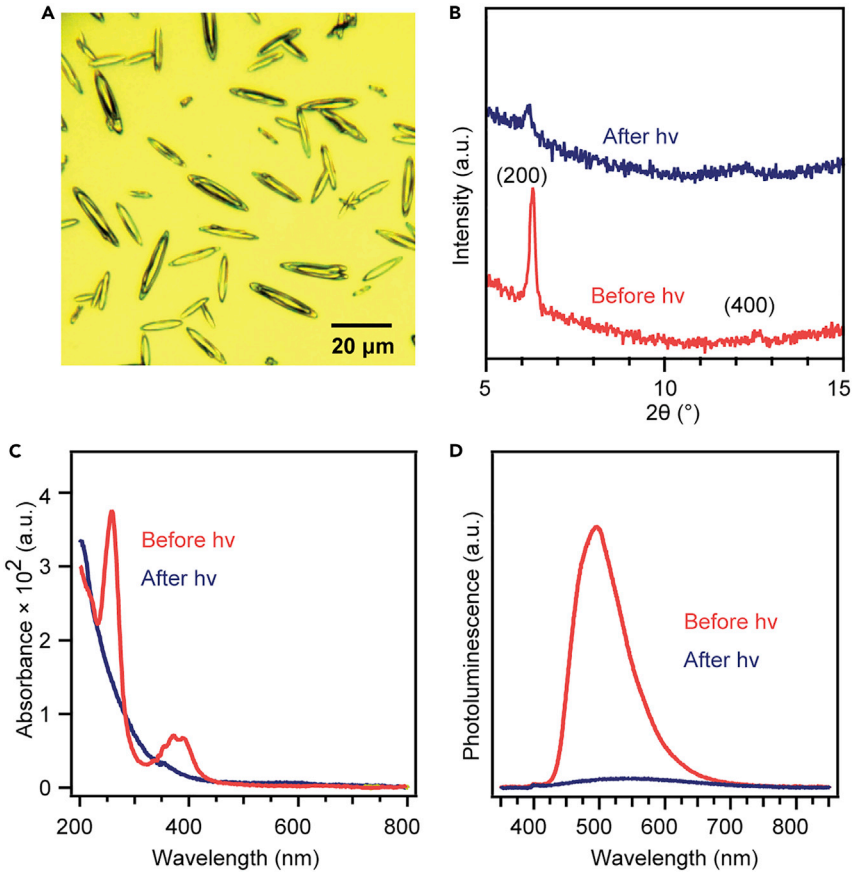

Figure 3. Characterization of MTBA and polyMTBA deposited on glass or quartz substrate

(A) Crystallites of **polyMTBA** on a glass substrate under optical microscope.

(B) Grazing-incidence X-ray diffraction pattern before and after irradiation, showing the (200) diffraction shifting to lower angle.

(C) UV-visible absorption spectra of **MTBA** deposited on quartz before and after irradiation.

(D) Photoluminescence spectra of the same sample as in (C).

helium atmosphere. The characteristic diffraction peaks of the polymer remain largely unchanged below 90°C, above which diffraction peaks start losing intensity (Figure 4A). Consistent with the VT-PXRD data, differential scanning calorimetry (DSC) of **polyMTBA** also reveals exothermic transformations with an onset temperature of approximately 100°C (Figure 4B), albeit displaying complexities that are in line with the behavior of previously reported 2D topochemical polymers.[29] Taken together, the VT-PXRD and DSC data pin 100°C as the onset of thermal depolymerization. NMR spectrum of the thermolyzed sample is identical to that of pristine **MTBA** (Figure S14), and the thermolysis product can be recrystallized to recover **MTBA** in the crystalline state (Figures 4C and 4D), which can be repolymerized (Figure S15). Under ambient conditions, minimal depolymerization is observed over weeks (Figure S16).

Conclusions

The foregoing results describe **polyMTBA**, a rare example of a 3D-connected, porous crystalline organic polymer. Enabled by topochemical photopolymerization, the formation of **polyMTBA** as a crystalline product is possible because crystallization of the monomers and the irreversible C–C bond formation between the

Please cite this article in press as: Sun et al., Reversible topochemical polymerization and depolymerization of a crystalline 3D porous organic polymer with C–C bond linkages, Chem (2022), https://doi.org/10.1016/j.chempr.2022.07.028

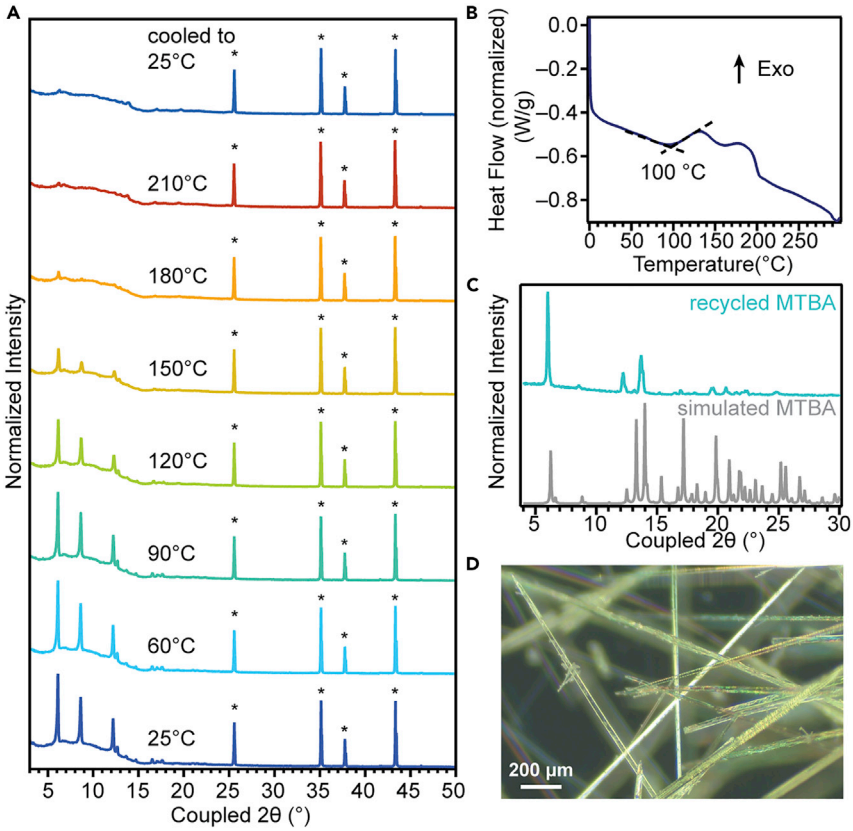

Figure 4. Thermal depolymerization of polyMTBA

(A) Variable-temperature powder X-ray diffraction patterns of **polyMTBA** under helium. Asterisks denote peaks from the alumina sample holder.

(B) The first heating trace of **polyMTBA** in differential scanning calorimetry. The onset of the exothermic event is at 100°C.

(C) Thermolyzed **polyMTBA** after recrystallization exhibits X-ray diffraction pattern similar to pristine **MTBA**. The difference in intensity is a result of strong preferred orientation, as the recrystallized **MTBA** forms long needles.

(D) Long needles of recrystallized thermolysis product under optical microscope.

monomers are decoupled. We show that topochemical dimerization of anthracene is possible despite a large C9···C10′ separation of 5.3–5.6 Å and that one-dimensional channels absent in the monomer crystals are created upon polymerization. The synthetic strategy introduced here enables the material to be recyclable and solution processable, thereby potentially serving as a blueprint for generating other complex and porous frameworks, including by exploiting co-crystallization and co-polymerization of dissimilar monomers.

EXPERIMENTAL PROCEDURES

Resource availability

Lead contact

Further information and requests for resources should be directed to and will be fulfilled by the lead contact, Mircea Dincă (mdinca@mit.edu).

Materials availability

All unique reagents generated in this study are available from the lead contact with a completed materials transfer agreement.

Data and code availability

Experimental and computational details and additional spectroscopic and crystallographic characterization data supporting findings in this paper are provided in the manuscript and supplemental information. Crystallography data of **MTBA** have been deposited at Cambridge Crystallographic Data Centre (CCDC: 2084357) and are publicly available as of the date of publication.

SUPPLEMENTAL INFORMATION

Supplemental information can be found online at https://doi.org/10.1016/j.chempr.2022.07.028.

ACKNOWLEDGMENTS

This work was supported by the National Science Foundation (NSF DMR-2105495). The high-resolution PXRD data were collected at 11-BM of the Advanced Photon Source at Argonne National Laboratory, which was supported by the U.S. Department of Energy, Office of Science, Office of Basic Energy Sciences, under contract no. DE-AC02-06CH11357. We are thankful to Prof. Marc Baldo and Dr. Dong-Gwang Ha for help with photoluminescence measurements.

AUTHOR CONTRIBUTIONS

C.S. and M.D. designed the experiments. C.S. executed the synthesis and characterization. C.S. and J.J.O. analyzed the adsorption data. G.S. performed crystallographic data collection and analysis. L.Y. collected and analyzed mass spectrometry data as well as analyzed nuclear magnetic resonance data. All authors contributed to writing of the manuscript and have given approval to the final version of the manuscript.

DECLARATION OF INTERESTS

The authors declare no competing interests.

Received: March 23, 2022
Revised: May 6, 2022
Accepted: July 28, 2022
Published: August 25, 2022

REFERENCES

1. Davankov, V.A., and Tsyurupa, M.P. (1990). Structure and properties of hypercrosslinked polystyrene—the first representative of a new class of polymer networks. React. Polym. *13*, 27–42. https://doi.org/10.1016/0923-1137(90)90038-6.

2. Côté, A.P., Benin, A.I., Ockwig, N.W., O'Keeffe, M., Matzger, A.J., and Yaghi, O.M. (2005). Porous, crystalline, covalent organic frameworks. Science *310*, 1166–1170. https://doi.org/10.1126/science.1120411.

3. Jiang, J.-X., Su, F., Trewin, A., Wood, C.D., Campbell, N.L., Niu, H., Dickinson, C., Ganin, A.Y., Rosseinsky, M.J., Khimyak, Y.Z., et al. (2007). Conjugated microporous poly(aryleneethynylene) networks. Angew. Chem. Int. Ed. Engl. *46*, 8574–8578. https://doi.org/10.1002/anie.200701595.

4. Ben, T., Ren, H., Ma, S., Cao, D., Lan, J., Jing, X., Wang, W., Xu, J., Deng, F., Simmons, J.M., et al. (2009). Targeted synthesis of a porous aromatic framework with high stability and exceptionally high surface area. Angew. Chem. Int. Ed. Engl. *48*, 9457–9460. https://doi.org/10.1002/anie.200904637.

5. Budd, P.M., Msayib, K.J., Tattershall, C.E., Ghanem, B.S., Reynolds, K.J., McKeown, N.B., and Fritsch, D. (2005). Gas separation membranes from polymers of intrinsic microporosity. J. Membr. Sci. *251*, 263–269. https://doi.org/10.1016/j.memsci.2005.01.009.

6. Kang, Z., Peng, Y., Qian, Y., Yuan, D., Addicoat, M.A., Heine, T., Hu, Z., Tee, L., Guo, Z., and Zhao, D. (2016). Mixed matrix membranes (MMMs) comprising exfoliated 2D covalent organic frameworks (COFs) for efficient CO 2 separation. Chem. Mater. *28*, 1277–1285. https://doi.org/10.1021/acs.chemmater.5b02902.

7. Doonan, C.J., Tranchemontagne, D.J., Glover, T.G., Hunt, J.R., and Yaghi, O.M. (2010). Exceptional ammonia uptake by a covalent organic framework. Nat. Chem. *2*, 235–238. https://doi.org/10.1038/nchem.548.

8. Liang, B., Wang, H., Shi, X., Shen, B., He, X., Ghazi, Z.A., Khan, N.A., Sin, H., Khattak, A.M., Li, L., et al. (2018). Microporous membranes comprising conjugated polymers with rigid backbones enable ultrafast organic-solvent nanofiltration. Nat. Chem. *10*, 961–967. https://doi.org/10.1038/s41557-018-0093-9.

9. Li, B., Zhang, Y., Ma, D., Shi, Z., and Ma, S. (2014). Mercury nano-trap for effective and efficient removal of mercury(II) from aqueous solution. Nat. Commun. *5*, 5537. https://doi.org/10.1038/ncomms6537.

10. Kaur, P., Hupp, J.T., and Nguyen, S.T. (2011). Porous organic polymers in catalysis: opportunities and challenges. ACS

Catal *1*, 819–835. https://doi.org/10.1021/cs200131g.

11. Xie, Y., Wang, T.-T., Liu, X.-H., Zou, K., and Deng, W.-Q. (2013). Capture and conversion of CO2 at ambient conditions by a conjugated microporous polymer. Nat. Commun. *4*, 1960. https://doi.org/10.1038/ncomms2960.

12. Lin, S., Diercks, C.S., Zhang, Y.-B., Kornienko, N., Nichols, E.M., Zhao, Y., Paris, A.R., Kim, D., Yang, P., Yaghi, O.M., et al. (2015). Covalent organic frameworks comprising cobalt porphyrins for catalytic CO_2 reduction in water. Science *349*, 1208–1213. https://doi.org/10.1126/science.aac8343.

13. Xu, F., Chen, X., Tang, Z., Wu, D., Fu, R., and Jiang, D. (2014). Redox-active conjugated microporous polymers: a new organic platform for highly efficient energy storage. Chem. Commun. *50*, 4788–4790. https://doi.org/10.1039/C4CC01002G.

14. Kou, Y., Xu, Y., Guo, Z., and Jiang, D. (2011). Supercapacitive energy storage and electric power supply using an aza-fused π-conjugated microporous framework. Angew. Chem. Int. Ed. Engl. *50*, 8753–8757. https://doi.org/10.1002/anie.201103493.

15. Lee, J.-S.M., Wu, T.-H., Alston, B.M., Briggs, M.E., Hasell, T., Hu, C.-C., and Cooper, A.I. (2016). Porosity-engineered carbons for supercapacitive energy storage using conjugated microporous polymer precursors. J. Mater. Chem. A *4*, 7665–7673. https://doi.org/10.1039/C6TA02319C.

16. DeBlase, C.R., Silberstein, K.E., Truong, T.-T., Abruña, H.D., and Dichtel, W.R. (2013). β-Ketoenamine-Linked Covalent Organic Frameworks Capable of Pseudocapacitive Energy Storage. J. Am. Chem. Soc. *135*, 16821–16824. https://doi.org/10.1021/ja409421d.

17. Liu, W., Luo, X., Bao, Y., Liu, Y.P., Ning, G.-H., Abdelwahab, I., Li, L., Nai, C.T., Hu, Z.G., Zhao, D., et al. (2017). A two-dimensional conjugated aromatic polymer via C–C coupling reaction. Nat. Chem. *9*, 563–570. https://doi.org/10.1038/nchem.2696.

18. Xu, H., Tao, S., and Jiang, D. (2016). Proton conduction in crystalline and porous covalent organic frameworks. Nat. Mater. *15*, 722–726. https://doi.org/10.1038/nmat4611.

19. Zhang, Y., Guo, J., Han, G., Bai, Y., Ge, Q., Ma, J., Lau, C.H., and Shao, L. (2021). Molecularly soldered covalent organic frameworks for ultrafast precision sieving. Sci. Adv. *7*, eabe8706. https://doi.org/10.1126/sciadv.abe8706.

20. Liu, J., Han, G., Zhao, D., Lu, K., Gao, J., and Chung, T.-S. (2020). Self-standing and flexible covalent organic framework (COF) membranes for molecular separation. Sci. Adv. *6*. eabb1110. https://doi.org/10.1126/sciadv.abb1110.

21. Nguyen, H.L., Hanikel, N., Lyle, S.J., Zhu, C., Proserpio, D.M., and Yaghi, O.M. (2020). A porous covalent organic framework with voided square grid topology for atmospheric water harvesting. J. Am. Chem. Soc. *142*, 2218–2221. https://doi.org/10.1021/jacs.9b13094.

22. Ben, T., and Qiu, S. (2013). Porous aromatic frameworks: synthesis, structure and functions. CrystEngComm *15*, 17–26. https://doi.org/10.1039/C2CE25409C.

23. Das, S., Heasman, P., Ben, T., and Qiu, S. (2017). Porous organic materials: strategic design and structure-function correlation. Chem. Rev. *117*, 1515–1563. https://doi.org/10.1021/acs.chemrev.6b00439.

24. He, T., Geng, K., and Jiang, D. (2021). All sp2 carbon covalent organic frameworks. J. Trends Chem. *3*, 431–444. https://doi.org/10.1016/j.trechm.2021.03.008.

25. Wang, S., Li, X.-X., Da, L., Wang, Y., Xiang, Z., Wang, W., Zhang, Y.-B., and Cao, D. (2021). A three-dimensional sp 2 carbon-conjugated covalent organic framework. J. Am. Chem. Soc. *143*, 15562–15566. https://doi.org/10.1021/jacs.1c06986.

26. Hema, K., Ravi, A., Raju, C., Pathan, J.R., Rai, R., and Sureshan, K.M. (2021). Topochemical polymerizations for the solid-state synthesis of organic polymers. Chem. Soc. Rev. *50*, 4062–4099. https://doi.org/10.1039/d0cs00840k.

27. Matsumoto, A. (2003). Polymer structure control based on crystal engineering for materials design. Polym. J. *35*, 93–121. https://doi.org/10.1295/polymj.35.93.

28. Guo, Q.H., Jia, M., Liu, Z., Qiu, Y., Chen, H., Shen, D., Zhang, X., Tu, Q., Ryder, M.R., Chen, H., et al. (2020). Single-crystal polycationic polymers obtained by single-crystal-to-single-crystal photopolymerization. J. Am. Chem. Soc. *142*, 6180–6187. https://doi.org/10.1021/jacs.9b13790.

29. Kissel, P., Murray, D.J., Wulftange, W.J., Catalano, V.J., and King, B.T. (2014). A nanoporous two-dimensional polymer by single-crystal-to-single-crystal photopolymerization. Nat. Chem. *6*, 774–778. https://doi.org/10.1038/nchem.2008.

30. Kory, M.J., Wörle, M., Weber, T., Payamyar, P., Van De Poll, S.W., Dshemuchadse, J., Trapp, N., and Schlüter, A.D. (2014). Gram-scale synthesis of two-dimensional polymer crystals and their structure analysis by X-ray diffraction. Nat. Chem. *6*, 779–784. https://doi.org/10.1038/nchem.2007.

31. Kissel, P., Erni, R., Schweizer, W.B., Rossell, M.D., King, B.T., Bauer, T., Götzinger, S., Schlüter, A.D., and Sakamoto, J. (2012). A two-dimensional polymer prepared by organic synthesis. Nat. Chem. *4*, 287–291. https://doi.org/10.1038/nchem.1265.

32. Feng, X., and Schlüter, A.D. (2018). Towards macroscopic crystalline 2D polymers. Angew. Chem. Int. Ed. Engl. *57*, 13748–13763. https://doi.org/10.1002/anie.201803456.

33. Yamanaka, S., Kubo, A., Inumaru, K., Komaguchi, K., Kini, N.S., Inoue, T., and Irifune, T. (2006). Electron conductive three-dimensional polymer of cuboidal C60. Phys. Rev. Lett. *96*, 076602. https://doi.org/10.1103/PhysRevLett.96.076602.

34. Yamanaka, S., Kini, N.S., Kubo, A., Jida, S., and Kuramoto, H. (2008). Topochemical 3D polymerization of C 60 under high pressure at elevated temperatures. J. Am. Chem. Soc. *130*, 4303–4309. https://doi.org/10.1021/ja076761k.

35. Huang, N., Ding, X., Kim, J., Ihee, H., and Jiang, D. (2015). A photoresponsive smart covalent organic framework. Angew. Chem. Int. Ed. Engl. *54*, 8704–8707. https://doi.org/10.1002/anie.201503902.

36. Acharjya, A., Pachfule, P., Roeser, J., Schmitt, F.J., and Thomas, A. (2019). Vinylene-linked covalent organic frameworks by base-catalyzed aldol condensation. Angew. Chem. Int. Ed. Engl. *58*, 14865–14870. https://doi.org/10.1002/anie.201905886.

37. Jadhav, T., Fang, Y., Liu, C.-H., Dadvand, A., Hamzehpoor, E., Patterson, W., Jonderian, A., Stein, R.S., and Perepichka, D.F. (2020). Transformation between 2D and 3D covalent organic frameworks via reversible [2 + 2] cycloaddition. J. Am. Chem. Soc. *142*, 8862–8870. https://doi.org/10.1021/jacs.0c01990.

38. Bouas-Laurent, H., Desvergne, J., Castellan, A., and Lapouyade, R. (2001). Photodimerization of anthracenes in fluid solutions: (Part 2) mechanistic aspects of the photocycloaddition and of the photochemical and thermal cleavage. Chem. Soc. Rev. *30*, 248–263. https://doi.org/10.1039/b006013p.

39. Beaudoin, D., Maris, T., and Wuest, J.D. (2013). Constructing monocrystalline covalent organic networks by polymerization. Nat. Chem. *5*, 830–834. https://doi.org/10.1038/nchem.1730.

40. Ma, T., Kapustin, E.A., Yin, S.X., Liang, L., Zhou, Z., Niu, J., Li, L.-H., Wang, Y., Su, J., Li, J., et al. (2018). Single-crystal x-ray diffraction structures of covalent organic frameworks. Science *361*, 48–52. https://doi.org/10.1126/science.aat7679.

41. Bouas-Laurent, H., Desvergne, J., Castellan, A., and Lapouyade, R. (2000). Photodimerization of anthracenes in fluid solution: structural aspects. Chem. Soc. Rev. *29*, 43–55. https://doi.org/10.1039/a801821i.

42. Al-Kaysi, R.O., Müller, A.M., and Bardeen, C.J. (2006). Photochemically driven shape changes of crystalline organic nanorods. J. Am. Chem. Soc. *128*, 15938–15939. https://doi.org/10.1021/ja064535p.

43. Schmidt, G.M.J. (1971). Photodimerization in the solid state. Pure Appl. Chem. *27*, 647–678. https://doi.org/10.1351/pac197127040647.

44. Enkelmann, V. (1998). Single-crystal-to-single-crystal transformations: the long wavelength tail irradiation technique. Mol. Cryst. Liq. Cryst. Sci. Technol. A *313*, 15–23. https://doi.org/10.1080/10587259808044256.

45. Brancart, J., Van Damme, J., Du Prez, F., and Van Assche, G. (2020). Thermal dissociation of anthracene photodimers in the condensed state: kinetic evaluation and complex phase behaviour. Phys. Chem. Chem. Phys. *22*, 17306–17313. https://doi.org/10.1039/d0cp03165h.

46. Leskes, M., Madhu, P.K., and Vega, S. (2007). A broad-banded z-rotation windowed phase-modulated Lee-Goldburg pulse sequence for 1H spectroscopy in solid-state NMR. Chem. Phys. Lett. *447*, 370–374. https://doi.org/10.1016/j.cplett.2007.09.041.

47. Brown, S.P., Schnell, I., Brand, J.D., Müllen, K., and Spiess, H.W. (1999). An investigation of π-π packing in a columnar hexabenzocoronene

by fast magic-angle spinning and double-quantum 1H solid-state NMR spectroscopy. J. Am. Chem. Soc. *121*, 6712–6718. https://doi.org/10.1021/ja990637m.

48. Salzillo, T., and Brillante, A. (2019). Commenting on the photoreactions of anthracene derivatives in the solid state. CrystEngComm *21*, 3127–3136. https://doi.org/10.1039/C9CE00176J.

49. Salzillo, T., Zaccheroni, S., Della Valle, R.G., Venuti, E., and Brillante, A. (2014). Micro Raman investigation of the photodimerization reaction of 9-cyanoanthracene in the solid state. J. Phys. Chem. C *118*, 9628–9635. https://doi.org/10.1021/jp412484x.

50. Thommes, M., Kaneko, K., Neimark, A.V., Olivier, J.P., Rodriguez-Reinoso, F., Rouquerol, J., and Sing, K.S.W. (2015). Physisorption of gases, with special reference to the evaluation of surface area and pore size distribution (IUPAC Technical Report). Pure Appl. Chem. *87*, 1051–1069. https://doi.org/10.1515/pac-2014-1117.

51. Dubbeldam, D., Calero, S., Ellis, D.E., and Snurr, R.Q. (2016). RASPA: molecular simulation software for adsorption and diffusion in flexible nanoporous materials. Mol. Simul. *42*, 81–101. https://doi.org/10.1080/08927022.2015.1010082.

52. Reid, C.R., and Thomas, K.M. (1999). Adsorption of gases on a carbon molecular sieve used for air separation: linear adsorptives as probes for kinetic selectivity. Langmuir *15*, 3206–3218. https://doi.org/10.1021/la981289p.